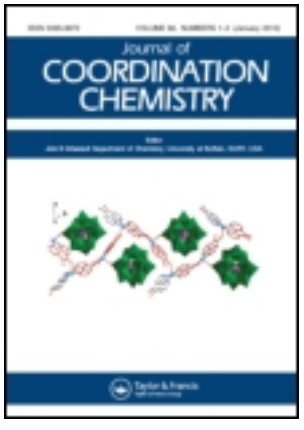

Journal of Coordination Chemistry
Publication details, including instructions for authors and subscription information:
http://www.tandfonline.com/loi/gcoo20

Three 3-amino-1,2,4-triazole-based cobalt(II) complexes incorporating with different carboxylate coligands: synthesis, crystal structures, and magnetic behavior

Xi-Ying Zhang[a], Zhong-Yi Liu[a], Yan-Fei Xia[a], Yan-Yan Zhang[a], En-Cui Yang[a] & Xiao-Jun Zhao[a]

[a] College of Chemistry, Tianjin Key Laboratory of Structure and Performance for Functional Molecules, Key Laboratory of Inorganic-Organic Hybrid Functional Material Chemistry, Ministry of Education, Tianjin Normal University, Tianjin, PR China

Published online: 10 Dec 2013.

To cite this article: Xi-Ying Zhang, Zhong-Yi Liu, Yan-Fei Xia, Yan-Yan Zhang, En-Cui Yang & Xiao-Jun Zhao (2013) Three 3-amino-1,2,4-triazole-based cobalt(II) complexes incorporating with different carboxylate coligands: synthesis, crystal structures, and magnetic behavior, Journal of Coordination Chemistry, 66:24, 4399-4414, DOI: 10.1080/00958972.2013.867023

To link to this article: http://dx.doi.org/10.1080/00958972.2013.867023

Journal of Coordination Chemistry, 2013
Vol. 66, No. 24, 4399–4414, http://dx.doi.org/10.1080/00958972.2013.867023

Three 3-amino-1,2,4-triazole-based cobalt(II) complexes incorporating with different carboxylate coligands: synthesis, crystal structures, and magnetic behavior

XI-YING ZHANG, ZHONG-YI LIU, YAN-FEI XIA, YAN-YAN ZHANG, EN-CUI YANG and XIAO-JUN ZHAO*

College of Chemistry, Tianjin Key Laboratory of Structure and Performance for Functional Molecules, Key Laboratory of Inorganic-Organic Hybrid Functional Material Chemistry, Ministry of Education, Tianjin Normal University, Tianjin, PR China

(*Received 12 March 2013; accepted 14 November 2013*)

Three 3-amino-1,2,4-triazole (Hatz)-based paramagnetic metal complexes, $\{[Co_2(Hatz)_2(nip)_2]\cdot H_2O\}_n$ (**1**), $[Co(atz)(nb)]_n$ (**2**), and $\{[Co_3(H_2O)_4(Hatz)_6(btc)_2]\cdot 11.5H_2O\}$ (**3**) (nip^{2-} = 5-nitroisophathalate, nb^- = *p*-nitrobenzolate, and btc^{3-} = 1,2,4-benzenetricarboxylate), were respectively prepared by introducing differently carboxylate-containing rigid coligands. All these complexes were structurally and magnetically characterized by single-crystal and powder X-ray diffractions, elemental analysis, FT-IR spectra, thermogravimetric and magnetic measurements. Complex **1** has a four-connected $CdSO_4$-type framework with binuclear subunits periodically extended by ditopic μ-N1, N3-Hatz and carboxylate-containing linkers. Tetrahedral Co^{II} ions in **2** are periodically interlinked into an undulated layer by anionic μ_3-N1,N2,N3-atz^- connectors with deprotonated nb^- spacers located on the both sides. By contrast, complex **3** is a centrosymmetric trinuclear molecule aggregated by six neutral μ-N1, N3-Hatz molecules. The structural difference of **1**–**3** is significantly due to the flexible binding modes adopted by triazolyl and carboxylate groups. Additionally, **1** exhibits a field-induced metamagnetic transition from an antiferromagnetic ordering to a weak ferromagnetic state resulting from the magnetic competition between triazolyl and carboxylate mediators. Instead, comparable antiferromagnetic couplings transmitted by cyclic triazolyl groups are observed in the nearest neighbors of **2** and **3**.

Keywords: 3-Amino-1,2,4-triazole; Paramagnetic metal complex; Crystal structure; Thermal stability; Magnetism

1. Introduction

Magnetic metal complexes have always attracted a great deal of attention and witnessed an impressive development, since they simultaneously display fascinating structures and intriguingly magnetic properties [1, 2]. Collecting paramagnetic transition metal ions (Mn^{2+}, Fe^{2+}, Co^{2+}, Ni^{2+}, Cu^{2+}, and so on) with appropriate bridging ligands through a bottom-up approach has becoming one of general strategies for the preparation of a magnetic sample [3]. Acting as a large family of versatile ligands to coordinate with spin carriers in selective bi-, tri- and tetradentate bridging modes, five-membered N-heterocyclic azoles

*Corresponding author. Email: xiaojun_zhao15@163.com

with two or more N donors separated by ring carbon atoms (imidazole, triazole, and tetrazole) and their abundant derivatives have been extensively employed as short magnetic mediators to construct novel magnetic metal complexes [4–17]. More interestingly, the structural and magnetic diversities of these polyazolyl-based magnetic entities can be significantly triggered by introducing different spin carriers and secondary mediators [3, 6, 10, 11]. For example, a series of Cu^{II}_4 cluster-based three-dimensional (3-D) coordination polymers with interesting framework connectivity have recently been obtained by varying the polycarboxylate-containing coligands [10, 18], which, resulting from the cooperate interactions of the multiple heterobridges, have displayed strong antiferromagnetic interactions with the coupling constant up to 206 cm^{-1} [10, 11]. In contrast to the isotropic magnetic systems, the magnetic samples containing anisotropic Co^{II} ion possess interesting pillared-layered architecture or mixed corner- and/or edge-sharing triangular magnetic lattices, and display field-induced multiple-step magnetic transitions [13, 14]. Obviously, the single-ion anisotropy, the spin-orbit coupling of the spin carriers, the coordination preference of the mixed magnetic mediators, and the diverse magnetic lattices generated by the paramagnetic ion and triazolyl group were found to significantly govern the magnetic behaviors. As the ongoing investigations on the ternary triazole-based magnetic entities [4–16], herein, 3-amino-1,2,4-triazole (Hatz) and three carboxylate-based coligands with different functionality and molecular topology (5-nitroisophathalate acid (H_2nip), *p*-nitrobenzoic acid (Hnb), and 1,2,4-benzenetricarboxylic acid (H_3btc)) were selected as mixed heterobridges to assemble with an anisotropic Co^{II} ion under controllable conditions. As a result, a four-connected $CdSO_4$-type framework with dimeric Co^{II}_2 subunits extended by ditopic μ-N1, N3-Hatz and carboxylate-containing connectors for **1**, a wavy layer constructed from tetrahedral Co^{II} ions and anionic μ_3-N1,N2,N3-atz^- ligands for **2**, as well as a centrosymmetric trinuclear oligomer for **3** were respectively generated, which were structurally and magnetically characterized. Structural determinations reveal that the flexible coordination modes of triazolyl and carboxylate moieties essentially tune the structural diversity of **1**−**3**. Additionally, the magnetic competition between the carboxylate and triazolyl mediators leads to a field-induced metamagnetic transition of **1** from an antiferromagnetic ordering to a ferromagnetic state. Instead, weak and comparable antiferromagnetic couplings are transmitted by a pair of triazolyl homobridges in the latter two complexes.

2. Experimental

2.1. *Reagents and instruments*

All chemicals were commercially purchased (3-amino-1,2,4-triazole, 5-nitroisophthalic acid, *p*-nitrobenzoic acid, and 1,2,4-benzenetricarboxylic acid were from Acros and other analytical-grade reagents were from Tianjin chemical reagent factory) and used as received without further purification. Elemental analyses for C, H and N were carried out with a CE-440 (Leeman-Labs) analyzer. Fourier transform (FT) IR spectra (KBr pellets) were taken on an Avatar-370 (Nicolet) spectrometer in the range 4000–400 cm^{-1}. Thermogravimetric analysis (TGA) experiments were performed on a Shimadzu simultaneous DTG-60A compositional analysis instrument from room temperature to 800 °C in N_2 atmosphere at a heating rate of 5 °C min^{-1}. Powder X-ray diffraction (PXRD) patterns were obtained from a Bruker D8 ADVANCE diffractometer at 40 kV and 40 mA for Cu Kα radiation (λ = 1.5406 Å), with a scan speed of 0.1 sec/step and a step size of 0.01° in 2θ.

The simulated PXRD patterns were calculated using single-crystal X-ray diffraction data and processed by the free Mercury v1.4 program provided by the Cambridge Crystallographic Data Center. Magnetic susceptibilities were acquired on a Quantum Design SQUID MPMS-XL-7 magnetometer with polycrystalline samples, in which the phase purity of the samples was determined by PXRD experiments. The magnetic susceptibility was corrected for the contribution of the gel capsule and for the core diamagnetism (using Pascal's constants).

2.2. *Synthesis of {[Co_2(Hatz)$_2$(nip)$_2$]·H_2O}$_n$ (1)*

A mixture containing $Co(NO_3)_2 \cdot 6H_2O$ (58.2 mg, 0.2 mmol), Hatz (25.2 mg, 0.3 mM) and H_2nip (21.0 mg, 0.1 mM) was dissolved in doubly deionized water (10.0 mL) and the initial pH value of the reactant mixture was adjusted to 6 by triethylamine. The resulting mixture was transferred into a Teflon-lined stainless steel vessel (23.0 mL) and heated at 130 °C for three days. After the mixture was cooled to room temperature at a rate of 4.4 °C h^{-1}, red block-shaped crystals of **1** suitable for X-ray analysis were obtained directly, washed with water and dried in air. Yield: 18.1 mg, 50% (based on H_2nip). Anal. Calcd for $C_{40}H_{32}Co_4N_{20}O_{26}$: C, 33.26%; H, 2.23%; and N, 19.39%. Found: C, 33.27%; H, 2.24%; and N, 19.41%. IR (KBr, cm^{-1}): 3442 br, 3357 br, 3088 w, 1653 s, 1615 s, 1533 s, 1457 m, 1432 m, 1381 s, 1349 s, 1283 m, 1226 m, 1083 w, 1055 w, 922 w, 783 w, 735 m, 719 m, 653 w, and 517 w.

2.3. *Synthesis of [Co(atz)(nb)]$_n$ (2)*

To an aqueous solution (6.0 mL) of $Co(NO)_3 \cdot 6H_2O$ (58.2 mg, 0.2 mM) was slowly added a methanol solution (4.0 mL) containing Hnb (16.6 mg, 0.1 mM) and Hatz (25.2 mg, 0.3 mM) with constant stirring and the initial pH value of the reactant mixture was adjusted to 7 by triethylamine. The resulting mixture was then transferred into a Teflon-lined stainless steel vessel (23.0 mL) and heated at 140 °C for three days. After the mixture was cooled to room temperature at a rate of 2.2 °C h^{-1}, purple block-shaped crystals of **2** suitable for X-ray analysis were obtained directly, washed with water and dried in air. Yield: 10.2 mg, 33% (based on Hnb). Anal. Calcd for $C_9H_7CoN_5O_4$: C, 35.08%; H, 2.29%; and N, 22.73%. Found: C, 35.07%; H, 2.28%; and N, 22.74%. IR (KBr, cm^{-1}): 3474 br, 3414 br, 3138 w, 1631 s, 1581 s, 1524 s, 1413 s, 1391 s, 1346 s, 1216 m, 1061 m, 1014 m, 881 m, 830 s, 792 m, 748 s, 719 m, 612 m, and 485 w.

2.4. *Synthesis of {[$Co_3(H_2O)_4$(Hatz)$_6$(btc)$_2$]·11.5H_2O} (3)*

To a methanol solution (4.0 mL) containing Hatz (25.2 mg, 0.3 mM) and H_3btc (21.0 mg, 0.1 mM) was dropwise added an aqueous solution (4.0 mL) of $Co(OAc)_2$ (49.0 mg, 0.2 mM) with constant stirring. The initial pH value of the resulting mixture was adjusted to 6 by triethylamine. The resulting mixture was filtered after further stirring for half an hour and the filtrate was undisturbed placed. Upon slow evaporation of the filtrate at room temperature, orange block-shaped crystals of **3** were generated in one week. Yield: 50.9 mg, 75% (based on Hatz). Anal. Calcd for $C_{15}H_{29.50}Co_{1.50}N_{12}O_{13.25}$: C, 26.56%; H, 4.38%; and N, 24.78%. Found: C, 26.52%; H, 4.40%; and N, 24.78%. IR (KBr, cm^{-1}): 3464 br,

3411 br, 3164 w, 1634 s, 1553 s, 1483 s, 1426 s, 1366 s, 1255 m, 1159 w, 1049 m, 982 w, 830 w, 776 w, 710 w, 621 w, 526 w, and 453 w.

2.5. *X-ray crystallography*

Diffraction intensities for **1-3** were collected on a Bruker APEX-II QUAZAR diffractometer equipped with graphite-monochromated Mo *Kα* radiation with a radiation wavelength of 0.71073 Å by using the *φ-ω* scan technique at 296 K for **1** and at 173 K for **2-3**. Semiempirical multi-scan absorption corrections were applied by SADABS, and the program SAINT was used for integration of the diffraction profiles [19]. The structures were solved by direct methods and refined with the full-matrix least-squares technique using the SHELXS-97 and SHELXL-97 programs [20]. The positions of hydrogen atoms bonded to carbon were generated geometrically and allowed to ride on their parent carbons before the final cycle of refinement. The H atoms of the water molecules except for the splitting water molecules were located from difference maps and refined with isotropic temperature factors. The oxygen atom of lattice water molecule in **1** (O7) is disordered with the site occupancy of 0.5. Five O atoms of free water molecules (O9, O11, O12, O13, and O14) in **3** are disordered: two, O9 and O11, varies between two positions with occupancies that refined to 0.644 for O9, 0.356 for O9′ as well as 0.553 for O11 and 0.447 for O11′; while the site occupancy for O12, O13 and O14 was respectively refined to 0.25, 0.75, and 0.25. The H atoms of the disordered water molecules in **3** were added as part of the model in idealized positions with riding thermal parameters. Detailed crystallographic data were summarized in table 1. Selected bond lengths and angles were given in tables 2–4, respectively. Hydrogen-bonding parameters were shown in table 5.

Table 1. Crystal data and structure refinements for **1**–**3**.[a]

	1	**2**	**3**
Formula	$C_{40}H_{32}Co_4N_{20}O_{26}$	$C_9H_7CoN_5O_4$	$C_{15}H_{29.50}Co_{1.50}N_{12}O_{13.25}$
Fw	1444.58	308.13	678.40
Crystal system	Monoclinic	Orthorhombic	Monoclinic
Space group	*C2/c*	*Pbca*	$P2_1/c$
a (Å)	15.7822(12)	8.5230(18)	9.8808(11)
b (Å)	12.7126(10)	10.524(2)	17.559(2)
c (Å)	12.7270(10)	25.448(5)	15.2064(17)
β (º)	103.7900(10)	90	94.748(2)
V (Å^3)	2479.9(3)	2282.6(8)	2629.2(5)
Z	2	8	4
D_{Calcd} (g cm^{-3})	1.935	1.793	1.714
μ (mm^{-1})	1.432	1.523	1.045
F (000)	1456	1240	1400
Limiting indices	$-18 \le h \le 18$	$-6 \le h \le 10$	$-6 \le h \le 11$
	$-15 \le k \le 15$	$-12 \le k \le 12$	$-20 \le k \le 20$
	$-8 \le l \le 15$	$-30 \le l \le 30$	$-18 \le l \le 17$
Data/restraints/params	2181/0/208	1984/0/172	4632/18/402
R_{int}	0.0144	0.0548	0.0579
GoF on F^2	1.054	1.054	1.051
R_1[a], wR_2[b] ($I > 2\sigma(I)$)	0.0245, 0.0663	0.0379, 0.0846	0.0671, 0.1684
R_1, wR_2 (all data)	0.0277, 0.0694	0.0526, 0.0932	0.1076, 0.1950
Residuals (e·Å^{-3})	0.313, – 0.334	0.389, – 0.489	1.649, − 0.849

[a] $R_1 = \Sigma(||F_o|-|F_c||)/\Sigma|F_o|$; [b] $wR_2 = [\Sigma w(|F_o|^2-|F_c|^2)^2/\Sigma w(F_o^2)^2]^{1/2}$.

Table 2. Selected bond lengths (Å) and angles (°) for **1**.[a]

Co(1)–O(2)[a]	2.0272(15)	Co(1)–N(1)[b]	2.1528(17)
Co(1)–O(1)	2.0555(14)	Co(1)–O(3)[c]	2.1809(15)
Co(1)–N(3)	2.1458(17)	Co(1)–O(4)[c]	2.2436(15)
O(2)[a]–Co(1)–O(1)	121.57(6)	N(1)[b]–Co(1)–O(3)[c]	87.63(6)
O(2)[a]–Co(1)–N(3)	87.61(7)	O(2)[a]–Co(1)–O(4)[c]	146.70(6)
O(1)–Co(1)–N(3)	89.97(6)	O(1)–Co(1)–O(4)[c]	91.60(6)
O(2)[a]–Co(1)–N(1)[b]	91.61(7)	N(3)–Co(1)–O(4)[c]	89.74(6)
O(1)–Co(1)–N(1)[b]	88.35(6)	N(1)[b]–Co(1)–O(4)[c]	92.26(6)
O(2)[a]–Co(1)–O(3)[c]	87.89(6)	N(3)–Co(1)–O(3)[c]	94.79(6)
O(1)–Co(1)–O(3)[c]	150.38(6)	O(3)[c]–Co(1)–O(4)[c]	59.27(5)

[a]Symmetry codes: [a] $-x, -y, 2-z$; [b] $x, -y, z+1/2$; [c] $x+1/2, y-1/2, z$.

Table 3. Selected bond lengths (Å) and angles (°) for **2**.[a]

Co(1)–N(2)	1.982(3)	Co(1)–N(3)[a]	2.013(3)
Co(1)–O(1)	1.989(2)	Co(1)–N(1)[b]	2.025(3)
N(2)–Co(1)–N(3)[a]	102.73(11)	O(1)–Co(1)–N(1)[b]	95.52(11)
O(1)–Co(1)–N(3)[a]	106.81(11)	N(3)[a]–Co(1)–N(1)[b]	110.97(11)
N(2)–Co(1)–N(1)[b]	103.87(11)	N(2)–Co(1)–O(1)	135.72(11)

[a]Symmetry codes: [a] $x+1/2, 1/2-y, 2-z$; [b] $1-x, 1-y, 2-z$.

Table 4. Selected bond lengths (Å) and angles (°) for **3**.

Co(1)–N(5)	2.115(5)	Co(2)–N(2)	2.071(6)
Co(1)–N(10)	2.127(5)	Co(2)–O(8)	2.084(5)
Co(1)–N(1)	2.153(5)	Co(2)–N(9)	2.095(5)
Co(2)–O(7)	2.141(5)	Co(2)–N(6)	2.108(5)
Co(2)–O(3)	2.152(5)	N(5)–Co(1)–N(1)	90.8(2)
N(5)–Co(1)–N(10)	90.3(2)	O(8)–Co(2)–N(6)	92.7 (2)
N(10)–Co(1)–N(1)	90.9(2)	O(7)–Co(2)–O(3)	85.82(19)
N(9)–Co(2)–N(6)	92.8(2)	O(8)–Co(2)–O(3)	88.2(2)
N(2)–Co(2)–O(7)	93.2(2)	N(2)–Co(2)–N(9)	89.9(2)
N(2)–Co(2)–N(6)	92.9(2)	O(8)–Co(2)–N(9)	92.1(2)
N(6)–Co(2)–O(7)	87.8(2)	O(8)–Co(2)–O(7)	84.8(2)
N(2)–Co(2)–O(3)	86.0(2)	N(9)–Co(2)–O(3)	93.6(2)

Table 5. Hydrogen-bonding parameters (Å, °) for **2** and **3**.[a]

Donor-H···Acceptor	D–H	H···A	D···A	D-H···A
1				
N2–H2′···O7	0.860	2.093	138.43	2.795
2				
N4–H4A···O4[a]	0.900	2.360	115.10	2.861
3				
N4–H4A···O2[a]	0.901	2.127	134.00	2.818
N11–H11A···O6[b]	0.880	1.815	157.28	2.648
N12–H12B···O5[c]	0.900	2.051	164.21	2.927
N7–H7···O2[d]	0.880	1.827	159.65	2.670

[a]Symmetry codes for **2**: [a] $1-x, y-1/2, 3/2-z$. For **3**: [a] $1-x, 1-y, -z$; [b] $2-x, y-1/2, -1/2-z$; [c] $2-x, y-1/2, -1/2-z$; [d] $1-x, y-1/2, 1/2-z$.

3. Results and discussion

3.1. *Syntheses and FT-IR spectra*

Two different preparation techniques, temperature-controlled solvothermal reactions for **1** and **2** as well as conventional evaporation method at room temperature for **3**, were applied for the successful preparations of the three targeted complexes. The initial pH value of the reaction mixture was carefully controlled to facilitate the coordination of the mixed ligands to metal ions by different deprotonation extent. As a result, single-crystal XRD structural determinations reveals that not only the organic acid coligands in **1-3** were fully deprotonated, the Hatz ligand in **2** was also in an anionic form, which was much different from the previous Hatz-based metal complexes [21, 22]. Additionally, the final crystalline products strongly depended on the anion of the inorganic cobalt source. NO_3^- for both **1** and **2** and OAc^- for **3** were found to be highly efficient for the growth of the crystalline products. Other common anions, such as ClO_4^-, Cl^- and OAc^- for **1** as well as ClO_4^-, Cl^- and SO_4^{2-} for **2**, can only lead to either clear solution or blue/green micro-crystals that can not be identified by single-crystal XRD determinations.

In the IR spectra (figure S1, see online supplemental material at http://dx.doi.org/10.1080/00958972.2013.867023), a pair of characteristic absorptions located at 3442 and 3357 cm^{-1} for **1**, 3474 and 3414 cm^{-1} for **2** as well as 3464 and 3411 cm^{-1} for **3** should be respectively ascribed to the stretching vibrations of N−H and/or O−H, revealing the coexistence of the amino group of Hatz and/or water molecule [23]. As compared with the free organic acids, the disappearance of a strong band respectively at 1717, 1690, and 1727 cm^{-1} for **1-3** is an indicative of the full deprotonation of H_2nip, Hnb and H_3btc. The strong bands between 1653 and 1346 cm^{-1} in **1-3** are resulting from the asymmetric (ν_{as}) and symmetry (ν_s) stretching vibrations of carboxylate groups. Thus, the IR results are in good agreement with those of single-crystal X-ray structural analysis.

3.2. *Structure descriptions of {[Co_2(Hatz)$_2$(nip)$_2$]·H_2O}$_n$ (1)*

Complex **1** exhibits a 3D four-connected $CdSO_4$-type framework with carboxylate aggregated binuclear subunits periodically extended by mixed Hatz and phenyl backbone of nip^{2-} connectors. The asymmetric unit of **1** contains one crystallographically unique Co^{II} atom, one neutral Hatz molecule, one doubly deprotonated nip^{2-} anion and one disordered lattice water molecule. As shown in figure 1(a), the sole Co^{II} ion in **1** is hexa-coordinated by four equatorial carboxylate O donors from three separate nip^{2-} coligands and two axial triazolyl N atoms from two individual Hatz molecules, adopting distorted octahedral coordination geometry. The Co–O distances are between 2.0272(15) and 2.2436(15) Å and the Co–N separations fall in the normal range of 2.1458(17) to 2.1528(17) Å (see table 2), which are comparable with those Co^{II}-based complexes with mixed carboxylate and tri-/tetrazolyl ligands [13, 14, 22]. Notably, the Co–O distances for the chelating carboxylate are obviously longer (ca. 0.1 Å) than those involved in the monodentate carboxylate, which is probably resulting from the spatially steric effect.

A pair of carboxylate groups from two symmetry-related nip^{2-} ligands hold two separate Co^{II} ions into a dimeric {$Co_2(COO)_2$} subunit with the intermetallic distance of 4.0688(3) Å (figure 1(b)), in which the conformation of the bridging carboxylate group is *μ-syn*, *anti*-COO^-. Previously, the *μ-syn*, *anti*-COO^- group belonging to 1,2,4,5-benzenetetracarboxylate ($btec^{4-}$) was also observed to bridge the adjacent Co^{II} ions into a 2D sublayer in the

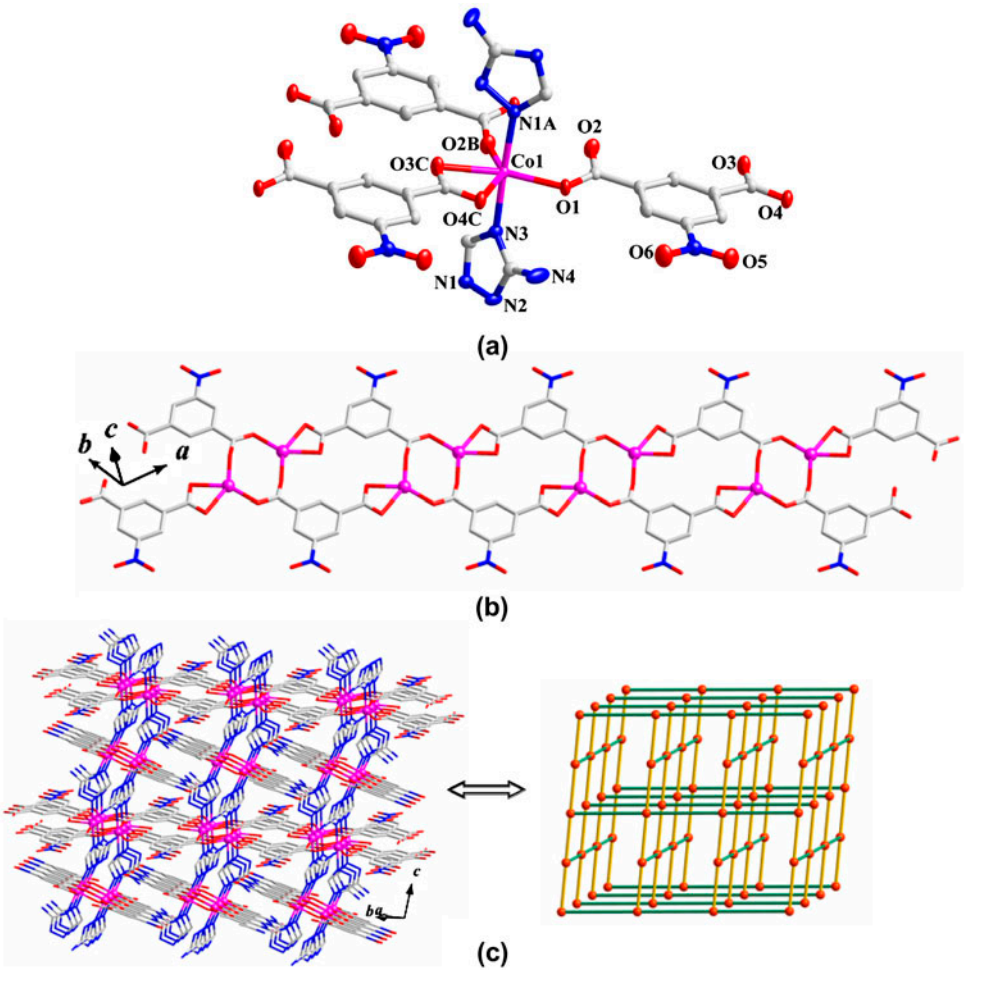

Figure 1. (a) Local coordination environments of Co^{II} ion in **1** (displacement ellipsoids were drawn at the 50% probability level. H atoms were omitted for clarity, symmetry codes: A = x, $-y$, 0.5 + z; B = $-y$, 2 − z; C = x + 1/2, y − 1/2, z). (b) 1D broad ribbon of **1** constructed from Co^{II} ions and nip^{2-} ligands. (c) Extended 3D framework and the four-connected $CdSO_4$ topological network of **1**.

complex $[Co(Hdatrz)_{0.5}(H_2O)_2(btec)_{0.5}]_n$ (Hdatrz = 3,5-diamino-1,2,4-triazole) [13] with the nearest Co^{II}…Co^{II} distance of 5.7391(2) Å, which is slightly longer than that in **1**. Each binuclear subunit of **1** can be further expanded by the phenyl backbone of nip^{2-} connector, leading to a one-dimensional (1D) Co^{II}-nip^{2-} broad ribbon respectively running along two orthogonal directions (figure 1b and 1c).

These broad ribbons are interconnected together by neutral μ-N1, N3-Hatz molecules to generate a robust 3D framework of **1** (figure 1c). The intermetallic distances spanned respectively by nip^{2-} and μ-N1,N3-Hatz mediators are 10.1327(6) and 6.3646(5) Å, which are almost beyond the magnetically interacting range. Thus, the dimeric $\{Co_2(COO)_2\}$ subunit would significantly dominate the magnetic couplings of **1**. Topologically, each binuclear subunit in **1** connects four adjacent neighbors by a pair of Hatz linkers and two nip^{2-} ligands and can be considered as a four-connected node, and the bridging μ-N1,

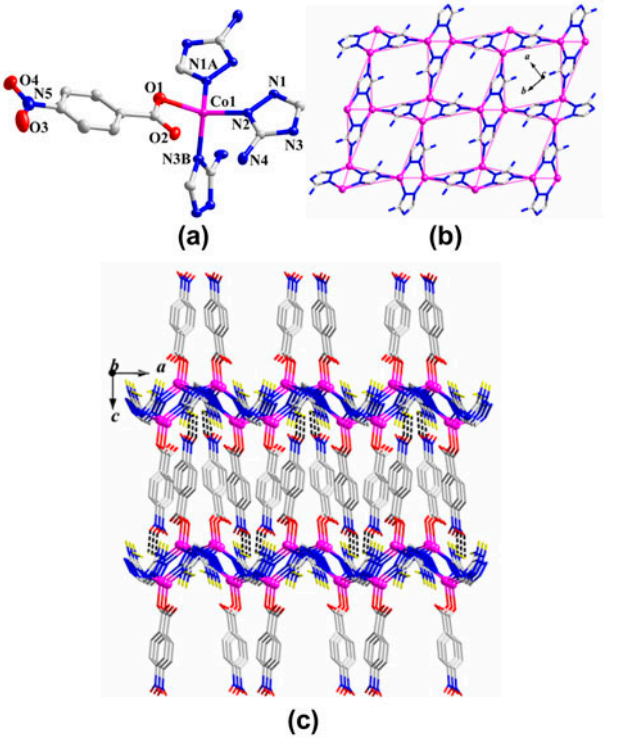

Figure 2. (a) Local coordination environments of Co^{II} ion in **2** (displacement ellipsoids were drawn at the 50% probability level. H atoms were omitted for clarity, symmetry codes: A = 1 − *x*, 1 − *y*, 2 − *z*; B = *x* + 1/2, 1/2 − *y*, 2 − *z*). (b) 2D (4.8^2) layer of **2** extended by μ_3-N1,N2,N4-atz^- connectors and the distorted Shastry-Sutherland magnetic lattice. (c) 3D supramolecular network of **2** formed by hydrogen-bonding interactions.

N3-Hatz and nip^{2-} ligands that connect with two dimeric subunits can be treated respectively as two differently ditopic linkers. Thus, the 3D framework of **1** can be predigested into a four-connected $CdSO_4$ topological network (figure 1(c)). Acting as an acceptor, the disordered lattice water molecule can produce an N-H···O hydrogen-bonding interaction with the amino group of Hatz ligand and interacts with the 3D framework of **1** (figure S2).

3.3. *Structure descriptions of [Co(atz)(nb)]$_n$ (2)*

Complex **2** is a bimetallic $\{Co_2(atz)_2\}^{2+}$ core-based (4.8^2) topological layer with terminally coordinated nb^- anion located on the both sides. The asymmetry unit of **2** contains one crystallographically independent Co^{II} cation, one deprotonated atz^- ligand and one deprotonated nb^- anion. Different from the octahedral metal site in **1**, the unique Co^{II} ion in **2** is four coordinated to one carboxylate O atom from one nb^- anion and three triazolyl N donors belonging to three symmetry-related atz^- ligands, assuming pseudo-tetrahedral coordination geometry with Co-O and Co-N separations falling in the normal range of 1.982(3)-2.025(3) Å (figure 2(a) and table 3).

Different from the neutral form in **1**, the Hatz ligand in **2** is in an anionic species and adopts a Y-shaped μ_3-N1,N2,N3 binding mode to aggregate separate Co^{II} ions in to an

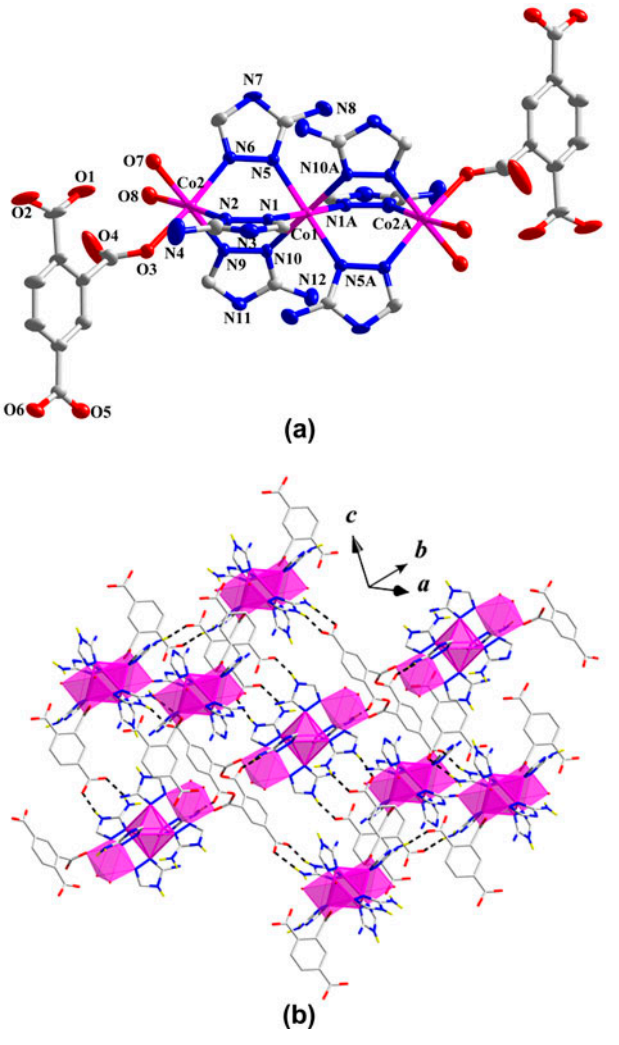

Figure 3. (a) Trinuclear structure of **3** (displacement ellipsoids were drawn at the 50% probability level. H atoms were omitted for clarity, symmetry codes: A = 1 – *x*, – *y*, – *z*). (b) 3-D supramolecular architecture of **3** generated by non-covalent interactions.

infinitely undulated (two-dimensional) 2-D layer with the monodentate nb^- coligands terminally located on the both sides. As shown in figure 2(b), two μ_3-N1,N2,N3-atz^- ligands hold a pair of symmetry-related spin carriers to generate a bimetallic $\{Co_2(atz)_2\}^{2+}$ subunits through the N1 and N2 positions and are further expanded the binuclear subunits together by the N3 donor bonding to the tetrahedral Co^{II} atom from the adjacent dimeric subunits. The $Co^{II}\cdots Co^{II}$ distances across the –NN– and –NCN– moieties of μ_3-atz^- are 3.8749(5) and 5.9706(1) / 6.0211(8) Å, which are comparable with those bridged by 3,5-diamino-1,2,4-triazole [13]. Notably, the adjacent $\{Co_2(atz)_2\}^{2+}$ subunits are perpendicular to each other generating a wavy 2D layer with (4.8^2) topology in the crystallographic *ab* plane. The tridentate binding fashion of the atz^- anion in **2** is much different from the bridging μ-N1,

N3– and μ-N1,N2-Hatz ligand in previously Hatz-containing metal complexes [22]. Obviously, due to the specific spatial arrangement of the atz^- ligands towards the Co^{II} atoms, the 2D sheet of **2** is wavy and contains repeated 16-membered macrocycles enclosed by four Co^{II} ions and four atz^- ligands. Magnetically, the connectivity of the spin carriers and anionic atz^- mediators affords a distorted Shastry-Sutherland magnetic lattice with competing antiferromagnetic interactions. The undulated 2D sheets in **2** give an –ABAB– staking sequence running along the crystallographic *c*-axis, leading to a 3D supramolecular architecture of **2** with the help of one N–H···O hydrogen-bonding interactions between the amino group of atz^- and the nitro moiety of the nb^- anions (figure 2(c) and table 5).

3.4. *Structure descriptions of {[$Co_3(H_2O)_4(Hatz)_6(btc)_2$]·11.5$H_2O$} (3)*

Complex **3** is a centrosymmetric trinuclear entity, which is infinitely stacked into a 3-D supramolecular network by weak intermolecular hydrogen-bonding interactions. The discrete oligomer of **3** includes three Co^{II} ions with Co1 atom located at an inversion center, six neutral Hatz ligands, four coordinated water molecules, two fully protonated btc^{3-} anions, as well as free and/or disordered water molecules. As shown in figure 3(a), the unique Co1 ion in **3** is surrounded by six triazolyl N atoms belonging to six separate Hatz molecules, displaying approximately perfect octahedral coordination geometry with the Co–N distances ranging from 2.115(4) to and 2.153(4) Å and the bond angles of ∠NCoN between 90.33(16) and 91.00(16)° (see table 4). Different from the coordination environment of Co1 atom, the Co2 site in **3** is in a N_3O_3 donor set completed by three individual Hatz molecules, one carboxylate group of btc^{3-} anion and two terminally coordinated water molecules, exhibiting distorted octahedral coordination geometry. The Co–N distances are between 2.071(6) and 2.108(5) Å (see table 4), which is considerable shorter than those involving the Co1 of **3**. The bond lengths of Co–O in **3** vary from 2.084(5) to 2.152(5) Å (see table 4), comparable with those in **1**.

The central Co1 and two centrosymmetric Co2 and Co2A sites are aggregated together by three pairs of bidentate bridging μ-N1, N2-Hatz ligands, giving rise to a linear trinuclear structure of **3** with the intermetallic separation of 3.7742(3) Å (figure 3a). The $Co^{II}\cdots Co^{II}$ separation in **3** is slightly shorter than that of **2** (3.8749(5) Å), but somewhat longer than those observed in $[Co_2(datrz)_2(nb)_2]_n$ (3.7017(6) and 3.5679(6) Å) [13] and $\{[Co_7(H_2O)_4(trz)_8(sip)_2]\cdot 3H_2O\}_n$ (3.6936(4) and 3.2708(3) Å, sip^{3-} = 5-sulfoisophthalate) [14] bridged by the $datrz^-$ and 1,2,4-triazolate (trz^-) ligands. The linear trinuclear entities are further connected with N–H···O hydrogen bonding interaction between the exocyclic amino/endocyclic imino moiety of Hatz ligand and the carboxylate group of btc^{3-} anion (table 5), leading to a 3D non-covalent network (figure 3(b)).

The above structural descriptions clearly reveal that the co-coordination of the deprotonated carboxylate and neutral/deprotonated 3-amino-1,2,4-triazole ligands can induce various interesting structures with different dimensionality and structural motifs, which can also be confirmed by other Co^{II}-containing coordination polymers with diverse carboxylate- [24–27] and/or triazolyl-modified [28, 29] ligands. For example, two 1D complexes with heterostranded double-helical chain and molecular ladder structure were respectively generated in the complexes of $[Co(mbtx)(hpht)(H_2O)]_n$ and $[Co(mbix)(hpht)]_n$ as a result of bridging role of hpht and mbtx ligands (mbtx = 1,3-bis(1,2,4-triazol-1-ylmethyl)benzene, mbix = 1,3-bis(imidazol-1-ylmethyl)benzene, H_2hpht = homophthalic acid) [30]. As compared to the three-atom carboxylate group, the N-heterocyclic triazole

ligand plays more important roles for the structural motifs and even the overall structures of **1**–**3**. The extended 3D framework of **1** is resulting from the cooperate binding of μ-N1, N3-atz$^-$ and μ-*syn*, *anti*-COO^- group of nip^{2-} anions. By contrast, the neutral μ_3-N1, N2, N3- and μ-N1, N2-Hatz ligand in **2** and **3** dominants essentially the connectivity modes of the adjacent metal ions. The different roles of the two mixed ligands have ever been reported in the Co^{II} and Cu^{II}-containing complexes with trz^- and benzenetricarboxylate/sulfoisophthalate anions [10, 11]. On the other hand, in contrast to the similar complexes with the two functional groups incorporated in the same ligand, the metal complexes with mixed ligands have more coordination flexibility and are responsible for the resulting structural diversity. For instance, acting as one of typically organic ligands with two coordinative moieties, 4-(1H-imidazol-1-yl) benzoic acid is modified by separate carboxylate and imidazolyl groups and expected to generate different metal complexes with structural diversity. Unfortunately, two previously reported 4-(1H-imidazol-1-yl) benzolate-based complexes with Zn^{II} and Co^{II} ions are isostructural, exhibiting 2D laminar layered structures with $M_2(CO_2)_2$ building blocks [31].

3.5. *PXRD patterns and thermal stability*

PXRD experiments have been carried out for **1-3** at room temperature to confirm their crystalline phase-purity and structural consistency. The experimental and computer-simulated PXRD patterns of the three bulk samples were in good agreement with each other (figure S3 in the Supplementary material), indicating the phase purity of the as-synthesized products. Thermogravimetric analyses (TGA) of **1**–**3** and free carboxylate-containing coligands were measured to evaluate their compositional stability (figure S4). As a result, complex **1** exhibits two separate weight-loss processes. The first one between 90 °C and 169 °C is due to the loss of the lattice water molecule (obsd: 2.5%, Calcd 2.8%). The second obvious weight-loss process that begins 283 °C and ends at 505 °C is ascribed to the removal of the mixed Hatz and nip^{2-} ligands, leaving CoO as final product of **1** (obsd: 19.2%, Calcd 20.8%). Notably, the weight-loss stage corresponding to the release of the mixed ligands can be roughly assigned to the decompositions of Hatz molecule (between 283 and 356 °C) and nip^{2-} (between 397 and 505 °C) anion, and the observed weight-loss value for the Hatz molecule is slightly different from that of theoretical one (obsd: 20.2%, Calcd 23.3%). Both **2** and **3** display a continuous weight-loss stage located in different temperature regions. Complex **2** is thermally robust up to 340 °C, and is accompanied by an apparent weight-loss stage, corresponding to the collapse of the layered motif. In contrast, **3** is thermal instability, and slowly broken down from room temperature to 800 °C. Obviously, complex **2** displays the highest thermal stability among the three complexes, although the Hnb ligand displays the lowest thermal stability of the three carboxylate-containing coligands (figure S4). Therefore, it can be concluded that the thermal stability of the targeted complexes may be more closely related to the polymeric structural nature.

3.6. *Magnetic properties*

Variable-temperature (2-300 K) magnetic susceptibilities of **1-3** were measured on the crystalline samples under an applied direct-current (dc) magnetic field of 2 kOe. As shown in figure 4(a), the $\chi_M T$ value for per Co^{II} ion of **1** is 2.70 cm^3 K M^{-1} at 300 K, which is much higher than the spin-only value (1.875 cm^3 K M^{-1}) expected for a high-spin octahedral

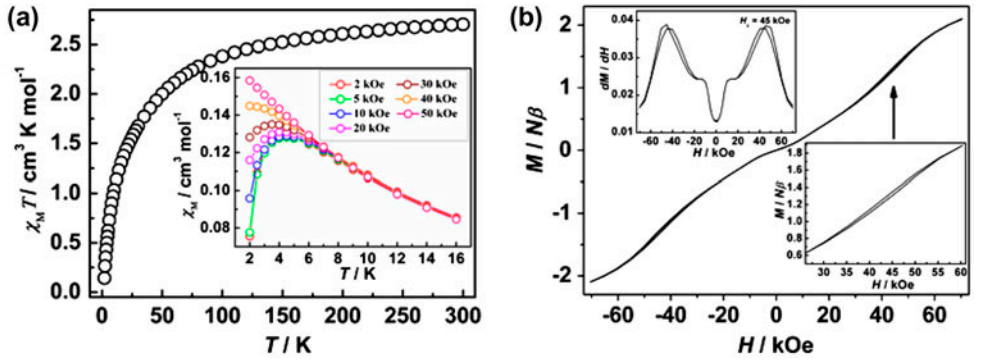

Figure 4. (a) Plot of $\chi_M T$ *vs.* T for **1** at 2 kOe (Insert: plots of χ_M *vs.* T under differently external magnetic fields at low temperature). (b) Field dependence of the magnetization of **1** at 2.0 K (Insert: the dM/dH *vs.* H derivative curve and magnified hysteresis loop).

Co^{II} ion with $S = 3/2$, $g = 2$ due to the large orbit contribution. As the temperature is lowered, the $\chi_M T$ product of **1** decreases continuously and reaches a value of 0.14 cm^3 K M^{-1} at 2.0 K. The curve of $\chi_M{}^{-1}$ *versus* T above 5.0 K obeys the Curie-Weiss law with $C = 2.88$ cm^3 K M^{-1} and $\theta = -20.3$ K (figure S5). Considering that the unquenched orbital-moment can contribute an artificial Weiss constant of –20 K for an isolated Co^{II} ion [1], the Weiss constant of **1** may indicate the existence of weak antiferromagnetic coupling or coexistence of the weak antiferro- and ferromagnetic interactions. The appearance of a round peak at 4.0 K in the χ_M *versus* T curve indicates an antiferromagnetic ordering (figure 4(a) inset). Interestingly, the peak at 4.0 K in the χ_M *versus* T curve disappears at an external field higher than 40 kOe (figure 4(a) inset), suggesting a magnetic phase transition from an antiferromagnetic ordering at a low field to a ferromagnetic state at a high field.

The field-dependent magnetization of **1** at 2.0 K reveals a sigmoid-shaped increase with the increased external magnetic fields (figure 4(b)), confidently confirming the metamagnetic behavior of **1**. The magnetization of **1** at the highest field (2.1 $N\beta$) is close to the product of one Co^{II} ion with $S = 1/2$ and $g = 4.1$–5.0, indicating a ferromagnetic state of **1** at higher field. The ferromagnetic state of **1** at higher field can be further convinced by two apparent hysteresis loops between 30 and 60 kOe (figure 4(b) insert). The critical field (H_c) of the metamagnetic transition is *ca.* 45 kOe determined by dM/dH curve. From the magnetostructural relationship, the magnetic behavior of **1** is dominated by two different bridges (μ-N1, N3-Hatz and *anti*, *syn*-COO^- of nip^{2-} ligand). The adjacent Co^{II} ions are ferromagnetic coupled through *anti*, *syn*-COO^- in the binuclear $\{Co_2(COO)_2\}$ subunits. And weak antiferromagnetic exchange interactions mediated by the μ-N1,N3-Hatz bridge can be coexist between the $\{Co_2(COO)_2\}$ units. Thus, the metamagnetism of **1** can be rationalized as a result of the competition between the two diverse superexchange pathways with different magnitude. Under a low external magnetic field, antiparallel alignment of the magnetic moments from the adjacent binuclear subunits can lead to an antiferromagnetic ordering. Once the external magnetic field exceeds *ca.* 45 kOe at low temperature, the weak interchain antiferromagnetic interactions mediated by μ-N1,N3-Hatz ligand can be overcome by the high field to lead to a ferromagnetic state of **1**. Compared with the previously reported metamagnet $[Co(Hdatrz)_{0.5}(H_2O)_2(btec)_{0.5}]_n$ (Hdatrz = 3,5-diamino-1,2,4-triazole, $btec^{4-}$ = 1,2,4,5-benzenetetracarboxylate) with $H_c = 22$ kOe [13]. The larger critical field of **1** should

attribute to the low dimensional magnetic structure, which essentially need higher external field to re-orientate the spins than $[Co(Hdatrz)_{0.5}(H_2O)_2(btec)_{0.5}]_n$. Additionally, the isostructural Mn^{II}-containing complex $\{[Mn_2(atz)_2(nip)_2]\cdot 2H_2O\}$ only exhibits typically antiferromagnetic interactions [22] essentially resulting from the different magnetic nature between Co^{II} and Mn^{II} ions.

The $\chi_M T$ product for each Co^{II} ion of **2** is 2.45 cm^3 K mol^{-1} at 300 K (figure 5), which is higher than those of one magnetically isolated spin-only tetrahedral Co^{II} ion with $g = 2.0$. Upon cooling, the $\chi_M T$ product undergoes a gradual decrease down to 0.09 cm^3 K M^{-1} at 2.0 K. The $\chi_M{}^{-1}$ *versus* T above 20.0 K obeys the Curie-Weiss law with $C = 2.67$ cm^3 K M^{-1} and $\theta = -29.4$ K. Obviously, such negative θ value represents the antiferromagnetic couplings between the nearest neighbors within the Shastry-Sutherland magnetic layer of **2** [10, 32]. The noncritical-scaling theory with the following simple phenomenological equation can be used to quantitatively fit the experimentally magnetic data from 300 to 2.0 K [33]:

$$\chi_M T = A\exp(-E_1/kT) + B\exp(-E_2/kT)$$

in which $A + B$ equals the Curie constant, E_1 and E_2 represent the "activation energies" corresponding to the spin–orbit coupling and the antiferromagnetic exchange interaction. The best fitted values obtained are as following: $A + B = 2.59$ cm^3 K M^{-1}, $E_1/k = 22.8$ K and $E_2/k = 4.58$ K. According to the relationship of $\chi_M T \propto \exp(J/2kT)$, the coupling constant between the spin carriers within the magnetic layer of **2** is –9.16 cm^{-1}, which well confirms the antiferromagnetic interactions. Previously reported complex $[Co_2(datrz)_2(nb)_2]_n$ with antiferromagnetically coupled Shastry-Sutherland magnetic lattice exhibit a spin-flop transition at higher fields, due to the coexistence of two unique tetrahedral Co^{II} ions with weak isotropy.

The $\chi_M T$ value of **3** at 300 K is 8.95 cm^3 K M^{-1} (figure 5), which is considerable higher than the spin-only value (5.62 cm^3 K M^{-1}) expected for three magnetically isolated Co^{II} ions with $S = 3/2$, $g = 2.0$ due to the large orbital contribution. Upon cooling, the product monotonously decreases to the minimum value of 1.71 cm^3 K M^{-1} at 2.0 K resulting from the spin-orbit coupling and the antiferromagnetic interactions between the adjacent Co^{II} ions. The $\chi_M{}^{-1}$ *versus* T data above 20 K follows the Curie-Weiss law with $C = 9.05$ cm^3 K M^{-1}

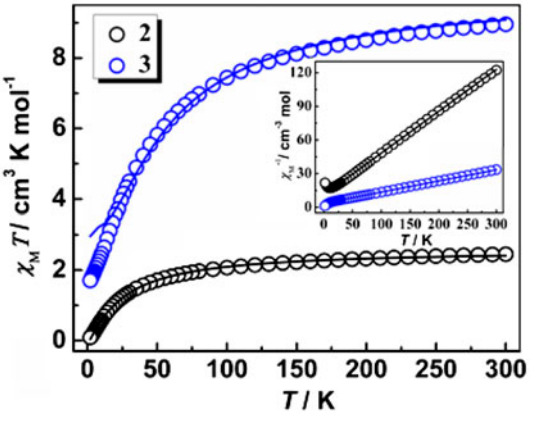

Figure 5. Temperature dependence of $\chi_M T$ and $\chi_M{}^{-1}$ for **2** and **3** (solid lines correspond to the best fit indicated in the text).

and θ = –36.1 K. The large negative value θ suggests a strong antiferromagnetic coupling between Co^{II} ions within the trinuclear unit. Structurally, complex **3** is actually an isolated linear trinuclear unit and affords a supramolecular network by weak hydrogen-bonding interactions. Therefore, the magnetic data of **3** between 20 and 300 K can be analyzed by an isotropic trimer model with the spin Hamiltonian $\boldsymbol{H} = -2J(\boldsymbol{S_1S_2} + \boldsymbol{S_2S_{1A}})$ and a molecule-field approximation. The resulting magnetic susceptibility equation is:

$$\chi_{Coi3} = \frac{2Ng^2\beta^2}{3KT}\left(\frac{\mathrm{A}}{\mathrm{B}}\right) \tag{1}$$

$$\mathrm{A} = 94\exp(-9J/KT) + 35\exp(-16J/KT) + 10\exp(-21J/KT) + 84\exp(-3J/KT) +$$

$$35\exp(-10J/KT) + 10\exp(-15J/KT) + \exp(-18J/KT) + 35\exp(-6J/KT)$$

$$+10\exp(-11J/KT) + \exp(-14J/KT) + 165$$

$$\mathrm{B} = 6\exp(-9J/KT) + 3\exp(-16J/KT) + 2\exp(-21J/KT) + 4\exp(-3J/KT)$$

$$+3\exp(-10J/KT) + 2\exp(-15J/KT) + \exp(-18J/KT) + 3\exp(-6J/KT)$$

$$+2\exp(-11J/KT) + \exp(-14J/KT) + 5$$

$$\chi_M = \frac{\chi_{Co3}}{1 - (2zJ'/Ng^2\beta^2)\chi_{Co3}} \tag{2}$$

The best-fit parameters are g = 2.33, J = –5.89 cm^{-1} and zJ' = –0.23 cm^{-1} with $R = 3.4 \times 10^{-3}$, where R is the agreement factor defined as $\Sigma[(\chi_M T)_{obsd}-(\chi_M T)_{Calcd}]^2/\Sigma[(\chi_M T)_{obsd}]$. The negative value J well confirms the moderate antiferromagnetic coupling of adjacent Co^{II} ions in the trimer and is close to other Co^{II} complexes bridging by 1,2,4-triazole [21, 34]. The zJ' component supports the weak inter-trimer antiferromagnetic contacts through abundant hydrogen bonds. On the other hand, the coupling strength in the nearest neighbors of the discrete trinuclear structures bridged by 3-fold triazolyl bridges are also closed related the types of the spin carrier, in which the coupling constant in the Cu^{II}-containing magnetic sample $[Cu_3(atr)_6(Hbtc)_2(H_2btc)_2]\cdot 2H_2O$ (atr = 4-amino-1,2,4-triazole, btc^{3-} = 1,3,5-benzenetricarboxylate) [35] is more than 9 times as strong as that of **3**.

4. Conclusion

Three 3-amino-1,2,4-triazole-based magnetic samples, an extended four-connected $CdSO_4$-type framework, a polymeric (4.8^2) topological layer as well as a discrete trinuclear oligomer, have been successful isolated by changing the secondary carboxylate-containing ligands. The structural diversity of the three complexes is significantly directed by the cooperative coordination of nonlinear carboxylate and heterocyclic triazolyl groups to the metal

ions. The magnetic competitions from the triazolyl and carboxylate heterobridges induce a field-induced a metamagnetic transition of **1** from an antiferromagnetic ordering to weak ferromagnetic state. Typically antiferromagnetic interactions mediated by two-fold triazolyl groups were observed in **2** and **3**.

Supplementary material

Crystallographic data for the structures reported here have been deposited with the Cambridge Crystallographic data Centre (Deposition No. CCDC – 921022, 921024, and 921023 for **1-3**). These data can be obtained free of charge via www.ccdc.cam.ac.uk/conts/retrieving.html (or from the Cambridge Crystallographic Centre, 12 Union Road, Cambridge CB21EZ, UK; Fax: +441223 336033; e-mail: deposit@ccdc.cam.ac.uk).

Funding

This present work was financially supported by the National Natural Science Foundation of China [grant 21171129], [grant 21173157]; Tianjin Municipal Education Commission (2012ZD02), which are gratefully acknowledged.

References

[1] M. Kurmoo. *Chem. Soc. Rev.*, **38**, 1353 (2009).
[2] (a) X.-Y. Wang, Z.-M. Wang, S. Gao. *Chem. Commun.*, **281**, (2008); (b) J.-P. Zhang, Y.-B. Zhang, J.-B. Lin, X.-M. Chen. *Chem. Rev.*, **112**, 1001 (2012).
[3] Y.-F. Zeng, X. Hu, F.-C. Liu, X-H. Bu. *Chem Soc. Rev.*, **38**, 469 (2009).
[4] (a) J.-R. Li, Q. Yu, E.C. Sañudo, Y. Tao, X-H. Bu. *Chem Commun.*, **2602**, (2007); (b) W.-C. Song, J. Tao, T.-L. Hu, Y.-F. Zeng, X.-H. Bu. *Dalton Trans.*, **40**, 11955 (2011).
[5] (a) Y. Li, W.-Q. Zou, M.-F. Wu, J.-D. Lin, F.-K. Zheng, Z.-F. Liu, S.-H. Wang, G.-C. Guo, J.-S. Huang. *CrystEngComm*, **13**, 3868 (2011); (b) Y.-B. Lu, M.-S. Wang, W.-W. Zhou, G. Xu, G.-C. Guo, J.-S. Huang. *Inorg. Chem.*, **47**, 8935 (2008).
[6] (a) W. Ouellette, M.H. Yu, C.J. O'Connor, D. Hagrman, J. Zubieta. *Angew. Chem. Int. Ed.*, **45**, 3497 (2006); (b) W. Ouellette, J.R. Galan-Mascaros, K.R. Dunbar, J. Zubieta. *Inorg. Chem.*, **45**, 1909 (2006); (c) W. Ouellette, S. Jones, J. Zubieta. *CrystEngComm*, **13**, 4457 (2011); (d) W. Ouellette, A.V. Prosvirin, J. Valeich, K.R. Dunbar, J. Zubieta. *Inorg. Chem.*, **46**, 9067 (2007); (e) P.J. Hagrman, C. Bridges, J.E. Greedan, J. Zubieta. *J. Chem. Soc., Dalton Trans.*, 2901, (1999).
[7] (a) P.-X. Yin, J. Zhang, Y.-Y. Qin, J.-K. Cheng, Z.-J. Li, Y.-G. Yao. *CrystEngComm*, **13**, 3536 (2011); (b) P.-X. Yin, Z.-J. Li, J. Zhang, L. Zhang, Q.-P. Lin, Y.-Y. Qin, Y.-G. Yao. *CrystEngComm*, **11**, 2734 (2009); (c) P.-X. Yin, J.-K. Cheng, Z.-J. Li, L. Zhang, Y.-Y. Qin, J. Zhang, Y.-G. Yao. *Inorg. Chem.*, **48**, 10859 (2009).
[8] (a) M. Tabatabaee, M. Tahriri, Y. Ozawa, B. Neumüller, H. Fujioka, K. Toriumi. *Polyhedron*, **33**, 336 (2012); (b) M. Tabatabaee, B.M. Kukovec, M. Kazeroonizadeh. *Polyhedron*, **30**, 1114 (2011).
[9] W.-X. Zhang, X. Wei, Y.-Z. Zheng, X.-M. Chen. *Chem. Commun.*, 3804, (2009).
[10] (a) E.-C. Yang, Z.-Y. Liu, L.-N. Zhao, X.-J. Zhao. *CrystEngComm*, **13**, 5401 (2011); (b) E.-C. Yang, Y.-L. Yang, Z.-Y. Liu, K.-S. Liu, X.-Y. Wu, X.-J. Zhao. *CrystEngComm*, **13**, 2667 (2011); (c) E.-C. Yang, B. Ding, Z.-Y. Liu, Y.-L. Yang, X.-J. Zhao. *Cryst. Growth Des.*, **12**, 1185 (2012); (d) E.-C. Yang, Z.-Y. Liu, Y.-L. Yang, J.-Y. Wang, X.-J. Zhao. *Dalton Trans.*, 8513 (2011); (e) E.-C. Yang, Z.-Y. Liu, X.-Y. Wu, H. Chang, E.-C. Wang, X.-J. Zhao. *Dalton Trans.*, 10082 (2011).
[11] E.-C. Yang, Z.-Y. Liu, X.-J. Shi, Q.-Q. Liang, X.-J. Zhao. *Inorg. Chem.*, **49**, 7969 (2010).
[12] (a) Z.-G. Gu, Y.-F. Xu, X.-H. Zhou, J.-L. Zuo, X.-Z. You. *Cryst. Growth Des.*, **8**, 1306 (2008); (b) T.-W. Wang, D.-S. Liu, C.-C. Huang, Y. Sui, X.-H. Huang, J.-Z. Chen, X.-Z. You. *Cryst. Growth Des.*, **10**, 3429 (2010); (c) D.-S. Liu, Y. Sui, T.-W. Wang, C.-C. Huang, J.-Z. Chen, X.-Z. You. *J. Chem. Soc., Dalton Trans.*, 5301 (2012).
[13] E.-C. Yang, Z.-Y. Liu, T.-Y. Liu, L.-L. Li, X.-J. Zhao. *Dalton Trans.*, 8132 (2011).

[14] Z.-Y. Liu, B. Ding, E.-C. Yang, X.-J. Zhao. *Dalton Trans.*, 9611 (2012).
[15] (a) X.-B. Li, G.-M. Zhuang, X. Wang, K. Wang, E.-Q. Gao. *Chem. Commun.*, **49**, 1814 (2013); (b) Q.-X. Jia, Y.-Q. Wang, Q. Yue, Q.-L. Wang, E.-Q. Gao. *Chem. Commun.*, 4894, (2008); (c) P.-P. Liu, A.-L. Cheng, N. Liu, W.-W. Sun, E.-Q. Gao. *Chem. Mater.*, **19**, 2724 (2007).
[16] (a) A. Grosjean, N. Daro, B. Kauffmann, A. Kaiba, J.F. Létard, P. Guionneau. *Chem. Commun.*, **47**, 12382 (2011); (b) W.-T. Liu, J.-Y. Li, Z.-P. Ni, X. Bao, Y.-C. Ou, J.-D. Leng, J.-L. Liu, M.-L. Tong. *Cryst. Growth Des.*, **12**, 1482 (2012).
[17] L. Arai, M.A. Nadeem, M. Bhadbhade, J.A. Stride. *Dalton Trans.*, 3372 (2010).
[18] X.-L. Wang, W. Zhao, J.-W. Zhang, Q.-L. Lu. *J. Solid State Chem.*, **198**, 162 (2013).
[19] A.X.S. Bruker. *SAINT software Reference Manual*, Madison, WI (1998).
[20] G.M. Sheldrick. *Acta Cryst.*, **A64**, 112 (2008).
[21] Y.-Z. Tong, Q.-L. Wang, M. Si, J. Qi, S.-P. Yan, G.-M. Yang, P. Cheng, D.-Z. Liao. *Polyhedron*, **30**, 3151 (2011).
[22] E.-C. Yang, X.-Y. Zhang, X.-G. Wang, Z.-Y. Liu, X.-J. Zhao. *Polyhedron*, **53**, 208 (2013).
[23] K. Nakamoto. *Infrared and Roman Spectra of Inorganic and Coordination Compounds*, Wiley, New York (1986).
[24] M.-L. Liu, Y.-X. Wang, W. Shi, J.-Z. Cui. *J. Coord. Chem.*, **65**, 1915 (2012).
[25] X.-Q. Zhao, Y.-C. Li. *J. Coord. Chem.*, **66**, 937 (2013).
[26] Y.-L. Chen, J. Yang, J.-F. Ma. *J. Coord. Chem.*, **65**, 3708 (2012).
[27] X.-T. Zhang, L.-M. Fan, Z. Sun, W. Zhang, D.-C. Li, P.-H. Wei, B. Li, J.-M. Dou. *J. Coord. Chem.*, **65**, 3205 (2012).
[28] L. Tian, L. Yan. *J. Coord. Chem.*, **65**, 1600 (2012).
[29] H.-Y. Ge, Y. Yang, Y.-F. Peng, B.-L. Li, Y. Zhang. *J. Coord. Chem.*, **65**, 3372 (2012).
[30] J.-H. Zhou, Y. Wang, S.-N. Wang, T. Wang, Y.-C. Chen, G.-X. Liu. *J. Coord. Chem.*, **66**, 737 (2013).
[31] Q.-Y. Liu, J. Guo, Y.-L. Wang, J.-J. Wei, Y. Chen, C.-H. Hu. *J. Coord. Chem.*, **66**, 530 (2013).
[32] B.S. Shastry, B. Sutherland. *Physica*, **108B**, 1069 (1981).
[33] (a) J.M. Rueff, N. Masciocchi, P. Rabu, A. Sironi, A. Skoulios. *Eur. J. Inorg. Chem.*, **11**, 2843 (2001); (b) J.M. Rueff, N. Masciocchi, P. Rabu, A. Sironi, A. Skoulios. *Chem. Eur. J.*, **8**, 1813 (2002).
[34] M.H. Klingele, P.D.W. Boyd, B. Moubaraki, K.S. Murray, S. Brooker. *Eur. J. Inorg. Chem.*, **573**, (2006).
[35] E.C. Yang, C.H. Zhang, Z.-Y. Liu, N. Zhang, L.N. Zhao, X.J. Zhao. *Polyhedron*, **40**, 65 (2012).